





Article

Challenges of the Optimization of a High-Speed Induction Machine for Naval Applications [†]

Giampaolo Buticchi ^{1,2}, David Gerada ², Luigi Alberti ³, Michael Galea ^{1,2}, Pat Wheeler ^{1,2}, Serhiy Bozhko ^{1,2}, Sergei Peresada ⁴, He Zhang ^{1,2,*}, Chengming Zhang ⁵ and Chris Gerada ^{1,2}

¹ Key Laboratory of More Electric Aircraft Technology of Zhejiang Province, The University of Nottingham Ningbo China, Ningbo 315100, China; buticchi@ieee.org (G.B.); michael.galea@nottingham.edu.cn (M.G.); pat.wheeler@nottingham.ac.uk (P.W.); serhiy.bozhko@nottingham.ac.uk (S.B.); chris.gerada@nottingham.ac.uk (C.G.)

² Department of Electrical and Electronic Engineering, The University of Nottingham, Nottingham NG7 2RD, UK; david.gerada@nottingham.ac.uk

³ Department of Industrial Engineering, University of Padova, 35122 Padova, Italy; luigi.alberti@unipd.it

⁴ Automation of Electromechanical Systems and the Electrical Drives Department, National Technical University of Ukraine, Kyiv 03056, Ukraine; sergei.peresada@gmail.com

⁵ Department of Electrical Engineering, Harbin Institute of Technology, Harbin 150006, China; cmzhang@hit.edu.cn

* Correspondence: he.zhang@nottingham.edu.cn

† This paper is an extended version of our paper published in Gerada, D.; Xu, Z.; Golovanov, D.; Gerada, C. Comparison of electrical machines for use with a high-horsepower marine engine turbocharger. In Proceedings of the 25th International Workshop on Electric Drives: Optimization in Control of Electric Drives (IWED), Moscow, Russia, 31 January–2 February 2018; pp. 1–6, doi:10.1109/IWED.2018.8321383.

Received: 16 May 2019; Accepted: 17 June 2019; Published: 24 June 2019



Abstract: In several industrial sectors, induction machines are being replaced with permanent magnet based alternatives, owing to the potential for higher power density and efficiency. However, high-speed applications feature a wide flux-weakening region, where advanced induction machines could bring benefits in terms of system-level optimization. This paper gives an overview the technological challenges for high-speed drives with induction machines, materials, simulations and future challenges for the power electronics in these applications. The target application is a high-speed induction machine for a naval turbocharging system. The comparison with permanent magnet synchronous machines will demonstrate how the extended flux weakening operation effectively allows for a weight reduction of the overall system.

Keywords: induction machine; high speed electrical drive; pulse width modulated inverter; computer simulation of electrical machines

1. Introduction

Electrification of transport affords a great opportunity to address emission [1] and climate change issues [2]. While electrification to date has been mainly concerned with secondary systems, rapidly extending areas are those of the more electric engine and general electrified traction and drives. These have been internationally identified as key technology areas by all international transport agendas and research strategies including ACARE's FlightPath2050 [3], the United Kingdom's Low Carbon Vehicle Partnership's transport roadmaps [2] and several Chinese agendas including the twelfth and thirteenth five-year plans and other initiatives such as the 'ten cities—thousand vehicles' programmes. It is for example at the centre of the United Kingdom (UK)-based Aerospace Technology Institute's (ATI) current preoccupations, as given in their strategy refresh of July 2016. To emphasize

the magnitude of the opportunity, for the automotive industry, it is expected that approximately 40% of all vehicles globally will be electrified by 2025. In China alone, the market growth of plug-in electric vehicles (EVs) increased by almost 2000% between 2009 and 2015, while the Chinese government expects a nation-wide EV presence ranging upwards of 5 million EVs by 2020.

From an aerospace perspective, the emissions predictions due to jet fuels is growing at an alarming rate. It is estimated from ongoing market and research studies that electrification activities in aerospace will comprise an increase to approximately 50% of overall more electric aircraft (MEA) activities, in the next 10 years [4].

The marine industry on the other hand, aided by the industry-specific, lower importance given to weight and power density values, has long been experimenting with various forms of electrification, including the classical turbo-electrical system. Today it is expected that fully-electrical marine vehicles will comprise more than 50% of all world-wide vehicles by the year 2035.

At the heart of all this effort and push towards electrification is the electrical drive itself. The importance of controlled electric drives is well known through all sectors of the industry. Electrical drives and power electronics (PE) have become a very important and significant industrial sector, currently worth about RMB 200 billion worldwide [5]. Electric drives constitute the backbone of industrial automation and their diffusion has been constantly increasing in every field, especially in the transportation industry. In fact, the ever-growing push towards more responsible and sustainable transport is resulting in electrical systems becoming more and more important. The electrical drive is typically made up of an electrical machine, a power electronics converter, a controller and the associated control algorithms. While electric drive technology has made huge steps forward in the last few decades, however many challenges still lie ahead, including adding new functionalities, improving efficiency and most importantly for transport applications, improving compactness and integration as well as the overall reliability, increasing power density and ability to operate in extreme temperatures. Underlying all of this is the push towards lower costs. The technology is advancing rapidly and new developments in components and customer requirements need to be embraced quickly by all interested parties.

An important feature of all the above is the need for higher power densities of these drives. Higher power densities result in lower weight and lower energy consumption and so forth, and therefore are a much sought after aspect. Traditionally, this has been sought after by implementing ever-higher rotational operating speeds, automatically resulting and implying the need for machines that are inherently ideal for high rotational speed operations. Thus, the induction machine with its super-robust rotor structure and its controllability has been traditionally thought of as the ideal choice for such applications.

Recently however the spectacular advent of the permanent magnet synchronous machine (PMSM), with its incomparable torque density and excellent efficiency values has resulted in these machines becoming more and more popular and wide-spread in the quest for higher power densities [6]. Their excellent torque density values can result in similar power densities as a high speed, Induction Machine (IM) counterpart, albeit at a much lower speed than that of the IM system. All this is today resulting in a general perception and feeling in the industry that the end for IMs is nigh.

However, the reality is also that an electric drive cannot and must not be evaluated only on its power density values. In fact for transport applications, power density is only one of various important design objective functions. In all transport applications, reliability, efficiency, adaptability and controllability are all equally important. A very important aspect for electrical drives is also the natural inclination of response and operation against the required given cycle. For example in automotive applications, operation at extended ranges is extremely important for the whole system level. In a review from 2012 [7], the authors noted that for automotive application all technologies of electric machines, IM, PMSM, Reluctance motor (RM) and even some DC motors can be used. Whereas in 2012 75% of the manufacturers opted for IMs [7] for their wider speed range operation, the other machines presented some advantages. RM is cheap and very robust with the temperature,

which is advisable for automotive applications but the higher torque ripple and noise may constitute an issue. PMSM drives have been gaining significantly in popularity since 2012 with the advantage of higher efficiency [8], although they present a higher cost and a higher sensitivity to temperature. Tesla has recently introduced the permanent magnet AC machine for the Model 3 in 2017 [9]. However, the decision regarding the best technology has to take into account many system aspects, including the driving cycle [10], which for electric vehicles always has low-speed (urban) and high-speed (highway) phases.

In today's world, meeting several objective functions for an electrical drive, can only be achieved with system-level optimisation. No matter what the machine technology or the converter family is, the reality is that system-level optimisation is becoming the most practical way how to achieve all the required parameters. And it is here that the IM does make another 'spectacular' comeback. For example, for high-speed machines, where an extended operation range is envisaged, the requirements of a wide flux-weakening region make the optimization procedure much more complex than usually required for low-frequency application [11].

The contribution of the presenters of the first Workshop on Induction Machines, held at The University of Nottingham Ningbo China in 2018, are hereby collected in the present work with the aim of describing how the IM drive can be designed with advanced optimisation techniques that can finally guarantee appropriate performance at system level, as expected from the most advanced PM drive options today. Based on detailed literature reviews and the most recent advances in design and optimisation techniques, this paper strives to build a case for the continued utilisation of IM drives in today's world of transport electrification that is currently being dominated by more modern systems and drives such as the PM drive [12].

The paper covers the materials and methods used in induction machine in Section 2, the results are reported in Section 3; the conclusion is reported in Section 4.

2. Materials and Methods

This section presents a brief description of the components for high-speed machines for the laminations and the windings.

2.1. Electrical Steels

The most common choices for the laminations are Silicon alloys: Silicon Iron (SiFe) and Cobalt Iron (CoFe). The CoFe saturation point depends on the mechanical characteristics (annealing temperature): the better the characteristics, the lower the saturation point. Even at the optimal annealing (critical for the stability at high speed), the advantage of the CoFe is the significantly higher (20%) saturation point than the SiFe, that comes at the expenses of the higher cost. For high-speed application, the lower weight of the assembly can bring benefits at system level if compared to the SiFe solution.

In addition to the choice of the material, also the lamination plays a fundamental role for the reduction of the core losses. This is critical, because high-speed machines have high excitation frequency. Electrical Steels as thin as 0.05 mm with very low core-losses, tailored specifically for high frequency applications are commercially available [13].

Figure 1 compares the mechanical yield-strength and core-loss characteristics at 1 T 400 Hz of commercially available grades of SiFe and CoFe under their respective trade-names. Considering the particular application, lamination thickness thinner than 0.35 mm are used but this comes at the expenses of the reduced yield strength. The blue (◇) represent different commercially-available grades of Silicon Iron laminations. The brown (■) represent different commercially-available grades of Cobalt Iron laminations.

Research on Silicon still has proved that the content of Si is correlated with better magnetic performance of the material and that the optimal point is at 6.5% of Si. From the manufacturing perspective, such a content makes it impractical to realize thin laminations. By using Chemical Vapour Deposition (CVD) technique this manufacturing issue has been overcome. SiFe with higher Silicon

percentage is however brittle, that is undesired at high speed. For this reason, a gradient injection of the lamination can be adopted, by having higher Silicon concentration towards the edges (to reduce the high frequency loss) and lower concentration towards the center.

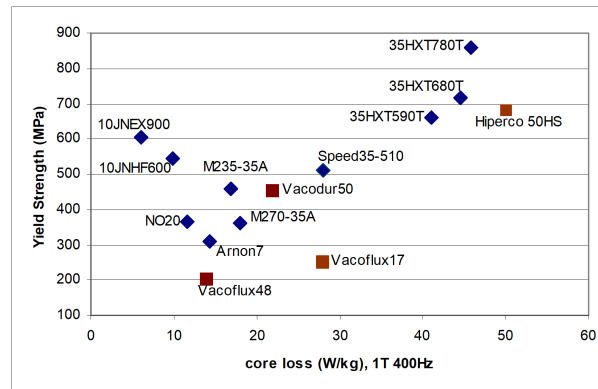


Figure 1. Comparison of core-losses and yield strength for different high-performance electrical steels (Reproduced from [14] with permission from IEEE).

The research related to the high-strength electrical steel has been recently very active due to the development of machines that feature bridges to guarantee the mechanical strength of the flux barriers (as interior permanent magnet machines or synchronous reluctance machines). The bridge should be designed to be as small as possible in order to not compromise the magnetic flux distribution. Techniques have been adopted to reach these aims [15].

2.2. Copper Alloys

A high-speed induction machine has strict requirements for the rotor bars and end rings:

- high yield strength
- high temperature
- high stiffness, to increase the critical speed
- high conductivity, to reduce the loss

The high temperature requirement rules out the usage of pure copper, that softens when the temperature increases. The solution is to create copper alloys without compromising the conductivity. Several different types of high strength copper alloys have been utilized for high speed induction machines, more typically Copper Zirconium (CuZr) [16] and Copper Aluminum Oxide (CuAl₂O₃) [17,18]. For the highest peripheral speeds, Copper Beryllium (CuBe) was traditionally considered the material of choice, despite its sensitivity in handling due to the toxic elements involved.

Figure 2 presents the different materials in an electrical conductivity/yield strength map. The blue (Δ) represent different commercially-available grades of pure copper and copper alloys. All other shapes refer to different high conductivity base materials (ex. silver, aluminum, steel etc.).

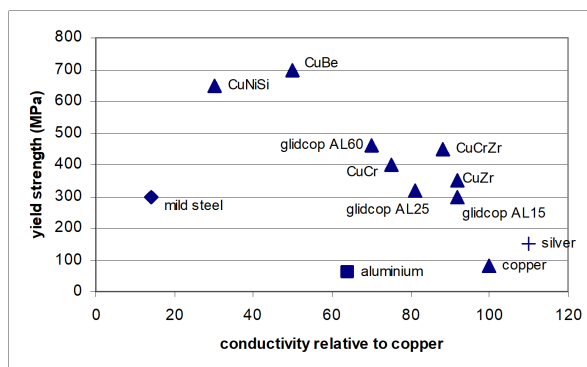


Figure 2. Comparison of losses and yield strength for different high-performance copper alloys (Reproduced from [14] with permission from IEEE).

2.3. Computation of IM Performance

The challenge of determining the performance of the IM has always attracted the attention of many researchers. Several different approaches have been proposed throughout the years considering analytical models and finite element computations. A precise performance evaluation is nowadays a mandatory goal for various reasons: international standards have dictated that industries produce more efficient electrical machines in order to reduce the global energy consumption. There is also an economic interest to increasing the power density of a machine: this means to reduce the machine dimensions for a given power and to increase the performance of a machine of given size. Best methods adopted today include thermal as well as electromagnetic analysis of the machine. This is certainly the case for machines operating in severe conditions, such as high-speed, high temperature, frequent overloads, corrosive or polluted atmosphere, and so on.

Besides these considerations, competition in the global marketplace has shortened the time frame in which new designs must be completed. In today's environment a very precise analysis which requires a long time is no longer acceptable, especially in an iterative design process with some parametrization or within an optimization cycle. When the finite element model of the motor is coupled with a complicated system model, the computational effort becomes not compatible with the industrial development process.

These facts then motivate the necessity for a rapid and accurate model for machine performance prediction. The model must be rapid enough for daily use in office routine calculation but yet has to exhibit reasonable accuracy.

The approach here presented consists of a combination of analytical and finite element methods in novel and original ways. Therefore, the speed of the analytical approach is refined with the accuracy of the finite element method and the synergy between the two methods is maximized [19–22]. Figure 3 shows the flowchart of the entire model.

Starting from the IM data and the operating conditions, a minimum set of Finite Element (FE) simulations is carried out to obtain the parameters of the equivalent circuit of the motor [20,21]. They are the no load magnetostatic simulations and locked rotor magneto-dynamic simulations.

Next, a lumped-parameter thermal model of the motor is built.

The magnetic model of the IM is based on the classical equivalent circuit shown in Figure 4 and Table 1 gives a description of the adopted variables. In the following, lowercase variables represent the normalized quantities, whereas uppercase ones refer to a specific machine.

In order to obtain an accurate prediction of the IM features, the equivalent circuit parameters have to be carefully computed. Hence, FE analysis is a mandatory choice. In order to limit the computational time, 2-D FE simulations are carried out and 3-D parameters are computed analytically and added to the equivalent circuit. To further increase the simulation speed, especially in design where a single lamination is shared among various motors, it is convenient to refer all the integral quantities that are derived from the FE analysis to a winding with one conductor per slot (i.e., $n_{cs} = 1$) and a unity stack

length (i.e., $L_{stk} = 1$ m). In this way, the result is independent of the voltage and the power rating of the actual motor.

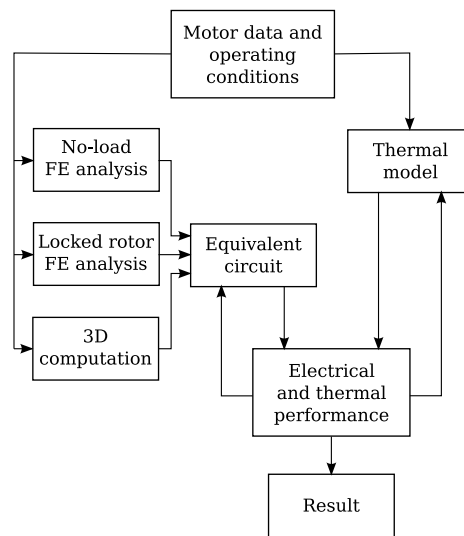


Figure 3. Combined electromagnetic-thermal analysis to compute the IM performance. The normalized equivalent circuit is coupled with a thermal model to update the machine parameters during analysis.

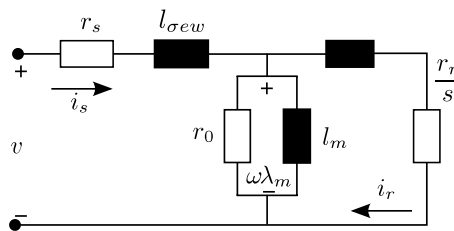


Figure 4. Normalized equivalent circuit (stack length 1m, one conductor per slot).

Table 1. Variable description for Figure 4.

r_s	Stator resistance
i_s	Stator current
v	Normalized Stator voltage
r_0	Resistor modeling iron loss
$l_{\sigma ew}$	Stator leakage resistance
l_m	Magnetizing inductance
λ_m	Stator flux
i_r	Rotor current referred to stator
r_r	Rotor resistance referred to stator
s	Slip

The resulting equivalent circuit is therefore normalized, that is, it is related to the lamination geometry and winding distribution rather than to a specific motor design. Its parameters are expressed as per unit quantities and can be easily scaled to any motor realized with the analysed lamination adjusting analytically the circuit parameters [21,22].

The FE analysis is 2-D; The following 3-D parameters are computed analytically and added to the equivalent circuit (Figure 5): (1) stator resistance; (2) stator coil end winding leakage inductance; (3) rotor cage ring resistance; and (4) rotor cage ring leakage inductance.

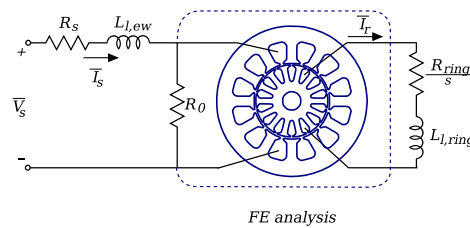


Figure 5. Combined analytical-FE analysis. 2D FE simulations are used to compute current and frequency dependent parameters in the circuit. 3D effects are accounted for analytically.

Once a lamination geometry has been simulated with these general FE simulations, the normalized equivalent circuit of Figure 4 can be computed. Then, the performance of any IM formed using the same lamination geometry and winding distribution can be achieved without further FE simulations simply by rearranging the normalized equivalent circuit analytically.

As an example, Figure 6 shows the torque versus slip characteristic of three IMs with different power ratings sharing the same lamination geometry. The different power ratings are achieved lengthening the stack and changing the number of conductors. Besides the torque characteristic, other relevant quantities, such as losses, power, efficiency and so on, can be computed with good agreement with experimental results. This simulation strategy has been profitably adopted to analyse and compute the performance of several three-phase and single phase IMs of various power ratings.

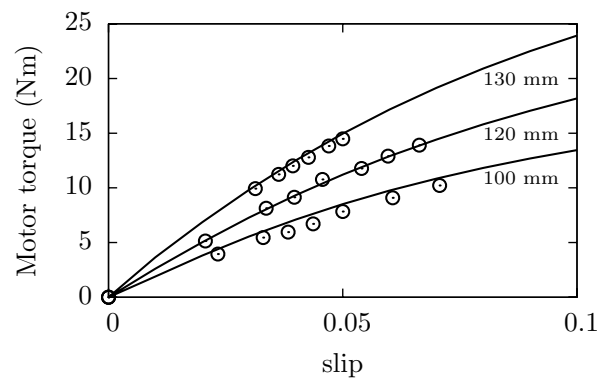


Figure 6. Torque vs slip for three IM of different power ratings (2.2, 3.0 and 3.7 kW) designed on the same lamination. Prediction (solid-line) and experimental measurements (circle marks) comparison.

The coupled thermal model is based on lumped parameters thermal network [23]. An example is shown in Figure 7 for an IM with a water jacket. A thermal model of the machine is particularly important when specific cooling system is adopted. This is the case, for example, of high power density machines. The thermal model is coupled with the electromagnetic one to update the parameters and to increase the accuracy of performance prediction. Thermal capacitance can also be included in the thermal model when dynamic behaviour has to be investigated. Both electric and thermal circuits are solved jointly in order to update each other iteratively [24].

Some other simulation techniques can be adopted in order to further improve the computation accuracy. For example it is possible to include eddy current losses in the lamination using homogenization techniques. Such additional effort requires an additional computational time but could be of interest in applications where iron losses become important. An example of such computational techniques applied to IM are reported in References [25,26].

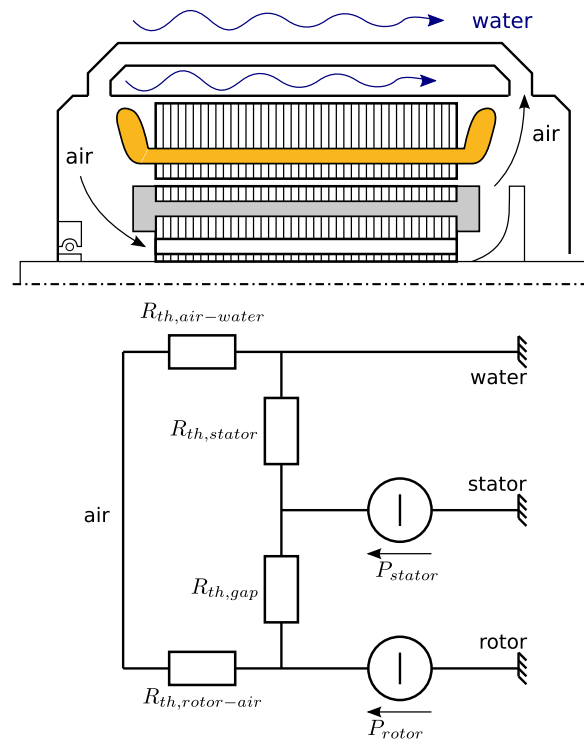


Figure 7. Example (simplified) of IM thermal model: thanks to the linearity of the problem a lumped-parameters thermal network can be profitably adopted. Some parameters in the network can be estimated via FE simulations (Reproduced from [23] with permission from IEEE).

2.4. Power Electronics

The main objective of the power electronics for a high-speed drive is to synthesize a low-distortion sinusoidal current waveform with high fundamental frequency. Considering that:

- the ratio between the switching and sampling frequency and the fundamental frequency constitutes one of the main control parameters for the drive,
- the switching frequency of the silicon power devices is limited, a high-speed drive is operating with a switching/fundamental ratio quite low. For the majority of the applications that rely on standard time-continuous control design, recommended values for this ratio is 15–20. This leads to switching frequencies in the order of 50 kHz for high-speed applications in the range of tens of kW.

In this framework, wide-bandgap devices have received increasing attention from both industry and academia because of their attractive characteristics in terms of low conduction and switching losses, higher thermal conductivity (for SiC), higher switching frequency capability and possible operation at higher temperatures. One of the first attempts towards the evaluation of wide-bandgap devices for electric drives was to substitute the silicon devices in the actual designs and evaluate the performance. Marked increase in the efficiency was demonstrated by several researchers [27], Figure 8. SiC MOSFETs showed also a better stability of their characteristics with increased temperature. Higher efficiency with the same operational parameters can be exploited either by reducing the cooling requirements or by increasing the switching frequency to decrease the size and cost of the magnetic components. In particular, if the same point of operation were chosen for both Si and SiC, the higher efficiency of the latter would lead to a reduced thermal stress and possibly longer lifetime.

It has been shown that with the advancement of the technology and of the increased market penetration of variable frequency drives, the concerns in terms of reliability are growing and special design procedures as the design for reliability based on the physics of failure approach are attracting the interest. In this framework, it has been already demonstrated that SiC devices can offer efficient and high switching frequency operation for the high-speed drives, however, how these characteristics

can be fully exploited depends on the machine itself. Among the possible failures of the electrical machines are the bearing faults and the stator insulation fault. The bearing faults can be accelerated by the high-frequency currents due to the common-mode PWM harmonics because of the capacitive coupling between the windings and the ground. Lower machine inductance and higher switching frequency, that represents the key aspects of high-speed drives, increase the magnitude of this current. A possibility to reduce the leakage current with a conventional power electronics topology is to employ an optimized modulation strategy [28]. In fact, considering a three-phase converter, there are 8 possible switching states: six active vectors ($V_1 - V_6$) and two zero vectors (V_7, V_8). Each vector implies a different value of common mode voltage and the commutation between one vector to the other causes high-frequency common mode voltage variation that originates the leakage current. A possibility to mitigate the phenomenon is to choose between vectors with the same common mode voltage. This normally leads to the avoidance of the zero vectors and to high switching harmonics in the motor current.

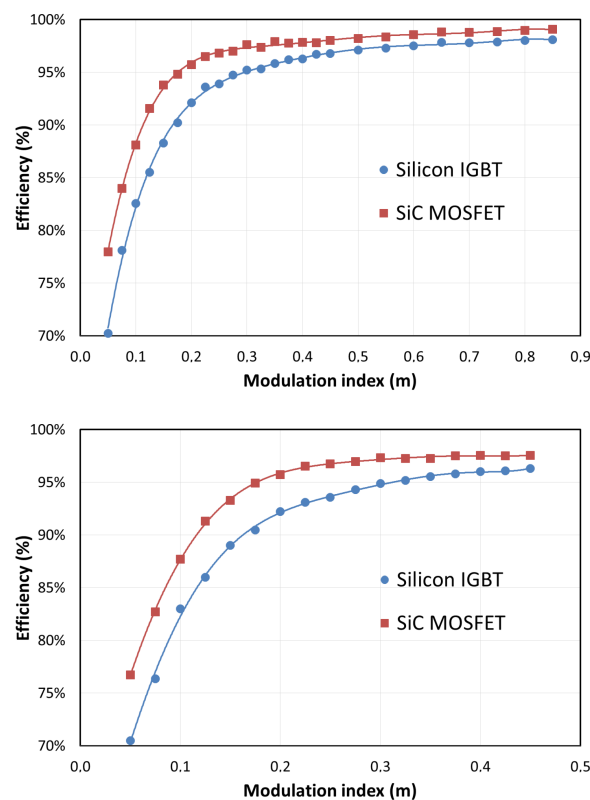


Figure 8. Efficiency improvement in the case of Si and SiC devices for the three-phase converter (top) and for the H8 architecture (bottom) (Reproduced from [27] with permission from IEEE).

Some topologies [29,30] tried to address the common-mode voltage generation with SiC power converter by modifying the three-phase bridge. This is shown in Figure 9, where additional devices are placed in the DC rails to decouple the DC and AC side of the converter during the free-wheeling phases. Proper space vector modulation ensures a reduction of the common-mode voltage. The peculiarity of this converter is that it allows to use the zero vectors with the same common mode voltage of the active vectors, as highlighted in Table 2, where the normalized output voltage (V_{uvwN}/V_{DC}) together with the normalized common mode voltage V_{CM}/V_{DC} of the conventional three-phase converter (H6) and the H8 converter is listed.

As discussed, the voltage stress causes the inter-turn insulation failure. Both the dv/dt and the switching frequency contribute to this effect and WBG-based drives for high-speed machines fall into this worst case for the machine. The basic problem is that the full characteristics of the WBG devices cannot be exploited if this leads to an over-designed machine in terms of insulation thickness

to meet the reliability requirements. Technological solutions to adapt the voltage stress depending on the design targets require the use of active gate drivers, as the one proposed in Reference [31], where the voltage and the current of the gate can be modified to control the dv/dt of a SiC MOSFET power module. An effective possibility to realize this voltage derivative control is shown in Figure 10, where an array of gate driver resistors is adopted, allowing to select among different transients. This would give the designers an additional degree of freedom to perform global converter/machine optimization. The reduced voltage stress of multi-level inverters could be exploited in this application to reduce the voltage stress of the electrical machines and, at the same time, improve the power quality and reduce the machine losses [32].

Table 2. Common-mode voltage (V_{CM}) values [30].

Vector	$\frac{V_{uN}}{V_{DC}}$	$\frac{V_{vN}}{V_{DC}}$	$\frac{V_{wN}}{V_{DC}}$	V_{CM}/V_{DC}	
				H6	H8
V_1	1	0	0	1/3	1/3
V_2	1	1	0	2/3	2/3
V_3	0	1	0	1/3	1/3
V_4	0	1	1	2/3	2/3
V_5	0	0	1	1/3	1/3
V_6	1	0	1	2/3	2/3
H6	V_7	0	0	0	0
	V_8	1	1	1	1
H8	V_7	1/3	1/3	1/3	1/3
	V_8	2/3	2/3	2/3	2/3

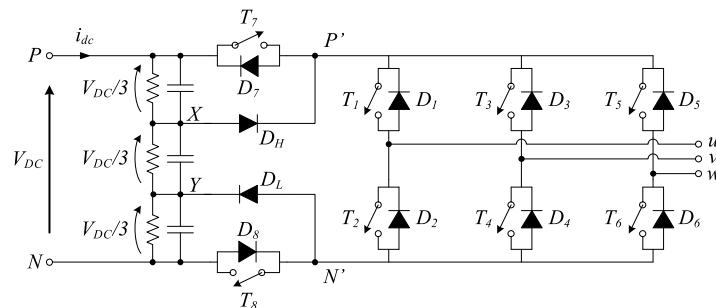


Figure 9. H8 converter based on the three-phase bridge for the common mode voltage reduction (Reproduced from [29] with permission from IEEE).

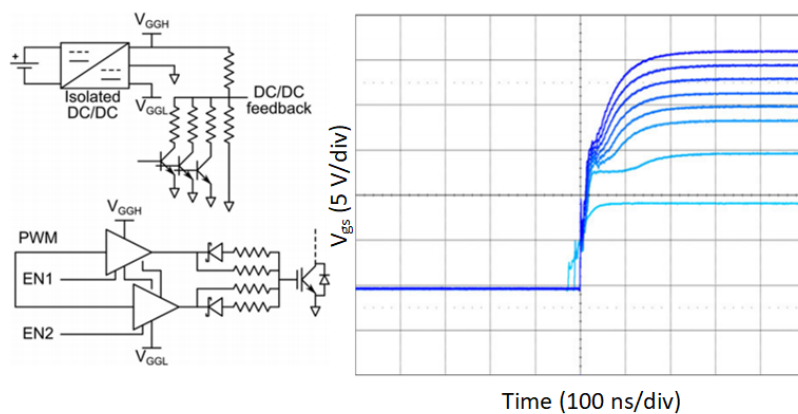


Figure 10. Possibilities for adaptive dv/dt (Reproduced from [31] with permission from IEEE).

3. Results and Discussion

In this section, an application example showing how an IM machine can constitute the optimal solution for a marine high-speed drive for Electrically-assisted turbocharging (EAT).

3.1. Application Description

Many published research on increased engine electrification focuses on the automotive spectrum of transportation [33,34]. However similar challenges exist with marine engines. For large vessels half of the total operational costs are fuel costs and ports worldwide are putting increasingly stringent legislations on emissions. High-efficiency propellers, engine waste-heat recovery and friction-reduction systems are among the researched technologies. With the recent first practical application and successful trials of a hybrid marine turbocharger on the freight ship Shin Koho [35,36], this technology is amongst the most promising to meet the emissions and fuel efficiency targets.

Within hybrid turbocharging, an electrical machine is placed on the same shaft as the compressor and turbine wheel of a turbocharger. On high engine loads, when there is high exhaust energy, the machine is used as a generator, and from the aforesaid trials on the Shin-Koho, it can continuously provide the vessels entire electrical load [35].

Under low-load operation, such as when slow-steaming, (<30% full-engine load), there is low energy in the exhaust, resulting in sub-optimal air-intake into the engine. In such instances, the electrical machine within the hybrid turbocharger can be used as a motor, replacing the traditional constant speed auxiliary air blower (typically a constant speed Induction Motor), thus resulting in lower electric power consumption and increased reliability.

The machine is 150 kW with a base speed of 25,000 r/min and a maximum speed of 50,000 r/min and is integrated between turbine and compressor. This translates to a Constant Power Speed Range (CPSR) of 2.

As a reference, a 3 MW marine engine is considered for the power-speed requirements. The minimum dimension for the airgap is set to be 0.5 mm and the engine coolant is used for the machine cooling as well.

While there are many electrical machine types, only a select few are capable of operating at very high speeds. A reliable starting guide is the r/min $\sqrt{\text{kW}}$ figure of merit [37], based on which the the Surface PM Machine and the laminated rotor IM are chosen as the topologies to be compared in more detail as shown in Figure 11. The candidates are the Permanent Magnet Synchronous Machine (PMSM) with Distributed Windings (DW) and Concentrated Windings (CW) and the Induction Machine.

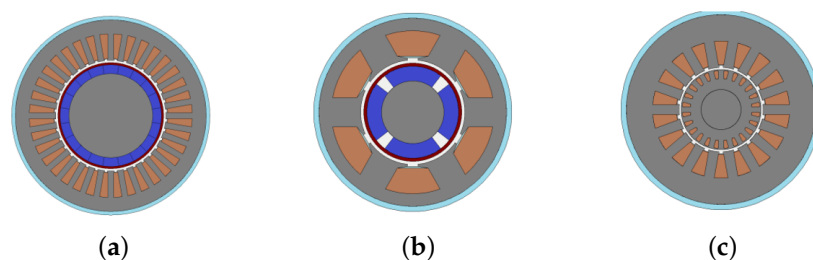


Figure 11. Machines selected for detailed EAT comparison: (a) Distributed Winding (DW) Surface PM, (b) Concentrated Winding (CW) Surface PM, (c) laminated IM.

Table 3 details the characteristics of the materials considered. All machine share the same kind of 0.1 mm JNEX laminations for the stator. For the rotor of the IM, 0.35 mm-thick high-strength HXT780T are employed. Insulation class C is considered for all machines.

Table 3. Electrical Machine Base Selection.

	SPM-DW	SPM-CW	IM
poles	4	4	2
slots	36	6	18 stator 24 rotor
stator lam.	10 JNEX	10 JNEX	10 JNEX
rotor lam.	-	-	HXT780T
other materials	Sm2Co17 Inconel718	Sm2Co17, Inconel718	CuCrZc CuCrZc

3.2. Machine Design

The torque-speed characteristic of the Surface- PM Machine is shown in Figure 12. Due to the lack of saliency, the field-weakening is severely limited and this implies higher power rating for the power electronics and an additional cost.

The intrinsic field control operation of the IM allows to easily meet the power-speed characteristics. However, the challenge lies in the materials, since high temperature, high conductivity and high strength copper must be used into the HXT780T laminations. For the configuration, 18 slots in the stator and 24 slots in the rotor are selected, the optimization technique proposed in Reference [17] is therefore applied. One of the key features is to use a drop-shaped bar instead of a circular one to increase the rotor current density.

The results of the thermal analysis are reported in Figure 13 for the PM and the IM machine at the rated power and base speed. The different sections are denoted as 'Sec 1-5', turbine and compressor are denoted by 'Turb' and 'Comp' whereas 'EW' denotes the end windings. Figure 13a shows the results for the CW surface PM. A very high temperature for the magnets is evident. Remarkably, a temperature gradient exists in the machine due to the high temperature of the turbine. Figure 13b is related to the IM and shows that a continuous rotor operation temperature of 360 C is achieved. The high thermal conductivity of the IM rotor helps averaging the rotor temperature, so no gradient is observed.

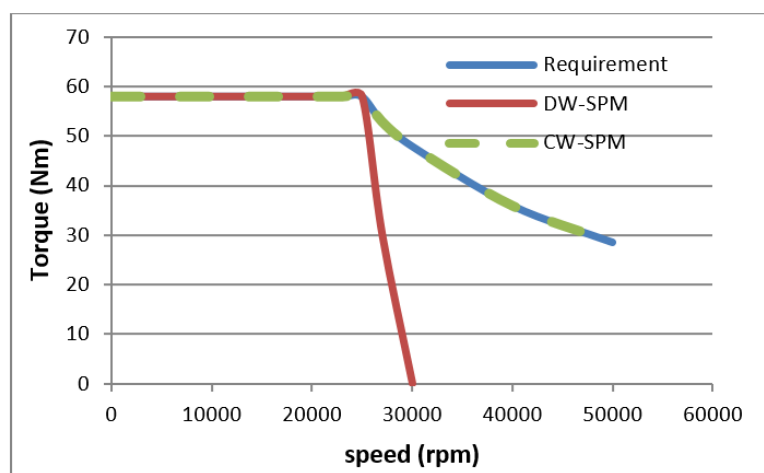
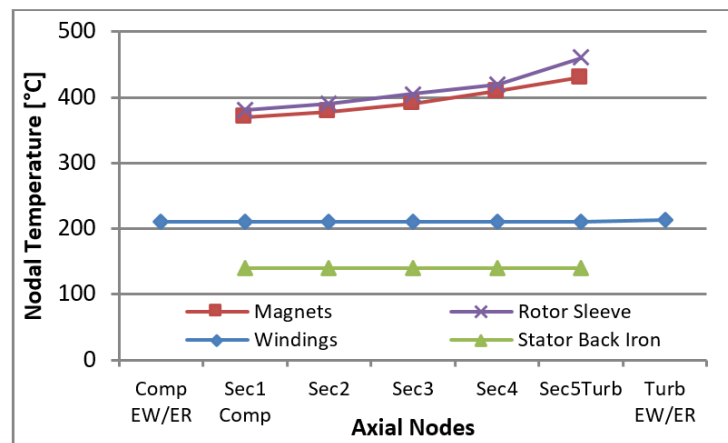
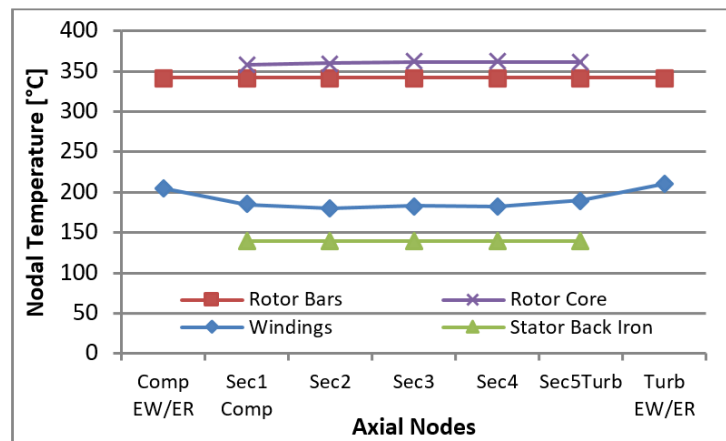


Figure 12. Torque-speed capability for DW Surface PM and Surface Inset PM Machines [38].



(a)



(b)

Figure 13. 36-slot, 4-pole CW Surface PM (a) and induction machine (b) nodal axial temperature distribution for magnets, rotor sleeve, windings and stator back iron (Reproduced from [38] with permission from IEEE). The x -axis represents the section of the machine where the temperature sensor was placed.

3.3. Cost Comparison, Overall Comparison and Selection

The comparison of the electrical machines considered in this analysis is shown in Table 4. As a note, only the efficiency of the machine without bearing and power electronics is considered. Since meeting the cost target is an important engineering task, also the cost analysis is performed. A constant cost for the power electronics of \$15/kVA is considered.

The permanent magnet machines must comply with the stringent requirement of maximum magnet temperature. The distributed-wound machine has a simple construction and presents the maximum efficiency among the selected electrical machine. From the temperature analysis, standard Sm2Co17 could be employed. However, the reduced field-weakening capability implies an increased size of the power electronics. The concentrated winding machine allows to meet the power-speed requirement thanks to a superior field weakening, however, as shown in Figure 13, the rotor temperature above 450 C is too high for the magnets. The construction of the Induction Machine is complex but it allows better value for money in achieving the performance target. The copper bars of

the rotor also contribute to making the rotor stiff and equalizing the axial temperature. After taking all the elements into consideration, the induction machine emerges as a winner for this application.

Table 4. Comparison between machine topologies for 150 kW EAT Application.

	DW SPM	CW SPM	IM
Electrical steel mass (kg)	15	13	21
Copper mass (kg)	5.8	6.6	9.1
Magnet/Copper Alloy mass (kg)	1.4	1.6	2.7
Torque Ripple (Nmpkpk)	1.6	4.1	6.2
Stator Cu loss (W)	1005	880	1380
Stator Fe loss (W)	1756	1799	1036
Rotor loss (W)	130	620	1404
Total Loss (W)	2891	3299	3820
Peak Rotor Temperature (C)	286	528	369
Inverter Rating (kVA)	330	184	186
Electrical Drive cost (\$/kW)	48.2	30.4	26.6

The prototyped 150 kW, 50,000 r/min induction machine is shown in Figure 14. A fabricated rotor is used instead of casting (that could be used for series production) and extrusion from solid CuCrZr is performed for the fabrication of the drop-shaped bars, which are inserted into the wire-cut rotor lamination stack. A silver alloy is used for brazing the copper bars to the end-rings.

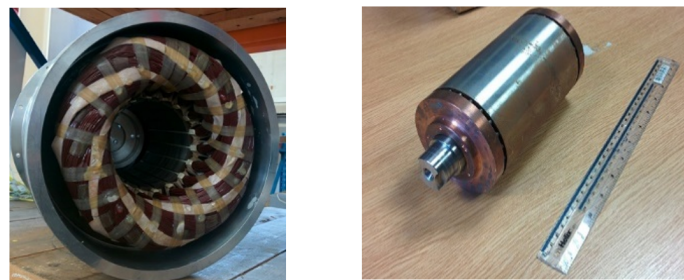


Figure 14. Prototyped 150 kW, 25,000–50,000 r/min high speed induction machine for marine EAT application (Reproduced from [14] with permission from IEEE).

3.4. Experimental Results

The first level of testing consists of performing the no-load and locked-rotor tests as described in IEEE112-2004 [39] standard, in order to obtain the equivalent circuit parameters shown in Figure 15. The parameters here are the stator resistance R_s , rotor resistance R_r , stator leakage reactance X_s , rotor leakage reactance X_r and the magnetizing reactance X_m .

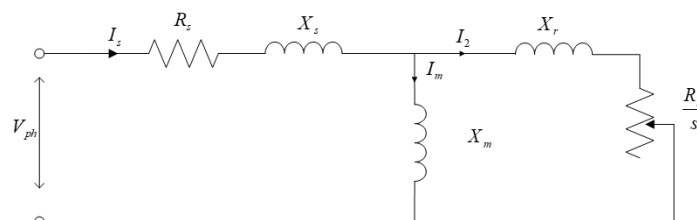


Figure 15. Induction Machine equivalent circuit [39].

In carrying out the no-load test, a variable frequency programmable supply, achieving almost pure sinusoidal waveforms is used. The supply frequency is increased in steps till the rated frequency. The reactive power of the motor at no load, Q_0 is calculated from:

$$Q_0 = \sqrt{(3V_0I_0)^2 - P_0^2} \quad (1)$$

where V_0 is the applied per-phase no-load rms voltage [V], I_0 is the no-load rms current [A] and P_0 is the no-load input power [W].

The total reactance at no-load X_0 is then calculated from :

$$X_0 = \frac{3V_0^2}{Q_0} \quad (2)$$

Referring to Figure 15, since the slip is 0 (or very small due to the no-load losses) at no-load, the reactance X_0 measured includes the stator leakage reactance X_s as well as the magnetizing reactance X_m .

$$X_0 = X_s + X_m \quad (3)$$

In order to compare the experimentally obtained magnetizing inductance with that predicted analytically as well as that obtained from the indirect FEA tests, the stator leakage component of the inductance, as computed analytically, $L_s = 0.1 \times 10^{-3}$ H, is subtracted from the experimental values. The results are summarized in Table 5, showing close matching between the three methods for the unsaturated values of magnetizing inductance.

Table 5. Magnetising inductance: measurement and prediction for unsaturated condition. Note: analytically obtained value of $L_s = 0.1 \times 10^{-3}$ H, subtracted from $L_m + L_s$ determined experimentally.

	L_m (H)
experimental (see note)	3.50×10^{-3}
analytical formulation	3.69×10^{-3} (+5.1%)
FE analysis	3.62×10^{-3} (+3.3%)

The rotor is then locked into position by suitable mechanical means as shown in Figure 16 and the locked rotor tests are performed. Simultaneous readings of voltage and current in all phases and of power input at several levels of voltage are taken in order to establish the value in the neighborhood of rated current. Referring to Figure 15, since the rotor is locked into position the slip is equal to 1. An approximate calculation of locked rotor impedance can be carried-out on the assumption that the magnetizing branch is open-circuited. Based on the aforesaid assumption, the rotor resistance R_r is estimated from :

$$R_r = \frac{P_L}{3I_L^2} - R_s \quad (4)$$

where P_L and I_L represent the power and the current measured from the locked rotor test. The total leakage reactance $X_s + X_r$ from:

$$R_r = \sqrt{\left(\frac{V_L}{I_L}\right)^2 - \left(\frac{V_L \cos \phi}{I_L}\right)^2} \quad (5)$$

where V_L , I_L are the phase voltage and current at locked rotor condition respectively. The comparison between the FEA and the experiment for the magnetizing inductance is shown in Table 6.

Table 6. Leakage inductance: measurement and prediction at rated current.

Method	$L_s + L_r$ (H)
experimental	0.00018
FE analysis	0.00016 (−11%)

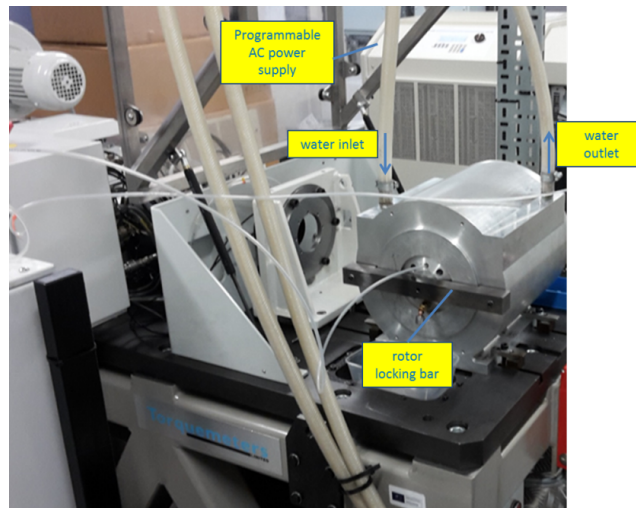


Figure 16. Locked rotor test setup on 150 kW IM.

The rotor resistance has been measured against the frequency and the result is shown in Figure 17. The orange line shows the actual experimentally-measured value of the rotor resistance and its increase with slip frequency due to skin effect. This is compared to the Finite-Element-Analysis (FEA) computed one (blue line) and the difference can be partially attributed to the temperature variation, since at high slip higher rates of heating are involved, and it is difficult to predict accurately the rotor temperature when the rotor resistance is measured.

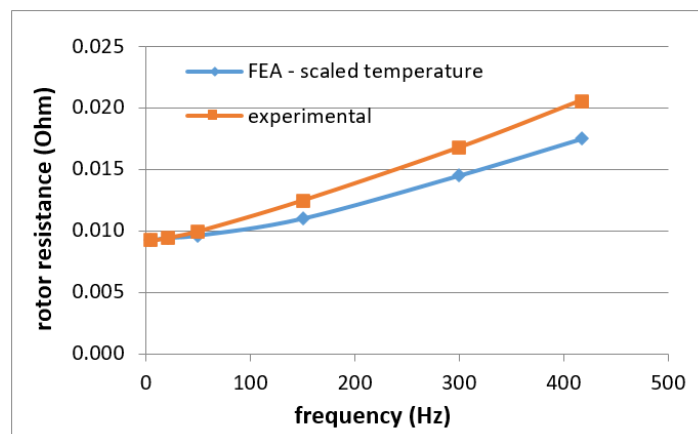


Figure 17. Rotor resistance variation with frequency: experimentally measured and FEA predictions.

The second level of testing is performed on a high speed dynamometer in order to check the performance on-load. In Figure 18 left, the measured current and torque are compared to the FEA predictions near the base speed of 25,000 r/min. Closer matching is observed at lower speeds (i.e., higher slip), due to the reduction of rotor slot leakage with the increased current. For a given speed the maximum difference between measured and predicted current is 9%. Figure 18 right shows similar experimental results near the maximum speed of 50,000 r/min.

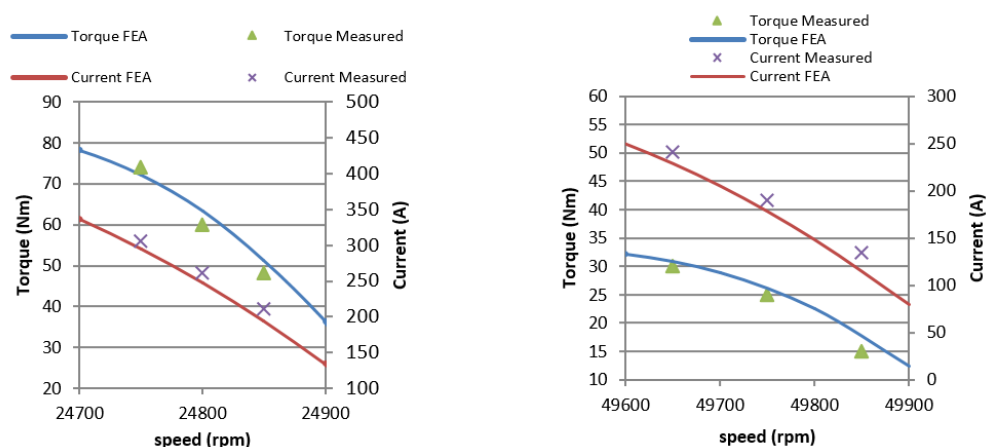


Figure 18. Comparison of measured and predicted performance near the base speed, 25,000 r/min, $f = 416$ Hz (left) and near the maximum speed, 50,000 r/min, $f = 833$ Hz (right) (Reproduced from [11] with permission from IEEE).

4. Conclusions

The induction machine has had a safe place in the global market because of its ease of use, reliable construction and low cost. The global changes in terms of industry modernization and the tight international regulation regarding the efficiency are pushing the designers towards new approaches.

In this manuscript, it has been shown how the induction machine, despite having lower rated efficiency than the permanent magnet or the synchronous machines, can still constitute the optimal solution for some high speed applications. Needless to be say, this kind of induction machine is not the low-cost/low-efficiency and easy to use kind that contributed to the success of this type of machine but it is a new design with high-performance materials and advanced power electronics. Although the traditional low cost machine is slowly being abandoned, these advanced design are just starting to make their appearance.

A case study for a high-performance naval application has been analyzed to support these statements and it has demonstrated that a solution based on an induction machine can outperform a solution based on permanent magnet machine. Although this result cannot have a general validity in the global context, it demonstrates that a holistic design that considers all the aspects of an electric drive must be performed to reach an optimized solution. To this aim, a comprehensive set of tools, including numerical simulation, finite element analysis, special power electronics must be considered.

Author Contributions: Investigation, G.B., D.G., L.A., M.G., P.W., S.B., S.P., H.Z., C.Z., C.G.; conceptualization, H.Z., P.W., C.G.; supervision, C.G., P.W.

Funding: This research was funded by the Ningbo Science & Technology Beauru under Grant 2017D10031, 2017D10029 and 2018B10002.

Acknowledgments: The authors would like to thank Cummins Generator Technologies (UK) for their continued support with high speed machine research, IBC Alloys (USA) for providing and supporting with advanced copper alloys, JFE Steel (Japan) for their support with low loss electrical steels and Nippon Steel Sumitomo Metal Corp. (Japan), for providing and supporting with high strength HXT780T electrical steel sheets.

Conflicts of Interest: The authors declare no conflict of interest.

Acronyms

EV	Electric Vehicle
PE	Power Electronics
IM	Induction Machine
PM	Permanent Magnet
PMSM	Permanent Magnet Synchronous Motor

RM	Reluctance Machine
EAT	Electrically-assisted Turbocharging
CVD	Chemical Vapour Deposition
WBG	Wide Band Gap
CPSR	Constant Power Speed Range
DW	Distributed Windings
CW	Concentrated Windings
FEA	Finite Elements Analysis
SVM	Space Vector modulation

References

- Partnership, L.C.V. *Transport Roadmap: A Guide to Low Carbon Vehicle, Energy and Infrastructure Roadmaps*; UK Department of Transport: London, UK, 2015.
- Needell, Z.A.; McNerney, J.; Chang, M.T.; Trancik, J.E. Potential for widespread electrification of personal vehicle travel in the United States. *Nat. Energy* **2016**, *1*, 16112. [[CrossRef](#)]
- European Commission. *Flightpath 2050: Europe's Vision for Aviation—Report of the High Level Group on Aviation Research*; European Commission: Brussels, Belgium, 2011.
- Bertolini, E.; Eury, S.; Hecker, P.; Huguet, M.; Sanna-Randaccio, F. *CLEAN SKY 2 Impact Assessment Final Report of the Expert Group*; Clean Sky 2 Joint Undertaking: Brussels, Belgium, 2012.
- Department for Business, Innovation & Skills. *The UK Power Electronics Industry: A Strategy for Success*; Department for Business, Innovation & Skills: London, UK, 2011.
- Duan, Y.; Ionel, D.M. A Review of Recent Developments in Electrical Machine Design Optimization Methods With a Permanent-Magnet Synchronous Motor Benchmark Study. *IEEE Trans. Ind. Appl.* **2013**, *49*, 1268–1275. [[CrossRef](#)]
- De Santiago, J.; Bernhoff, H.; Ekergrård, B.; Eriksson, S.; Ferhatovic, S.; Waters, R.; Leijon, M. Electrical Motor Drivelines in Commercial All-Electric Vehicles: A Review. *IEEE Trans. Veh. Technol.* **2012**, *61*, 475–484. [[CrossRef](#)]
- Rind, S.J.; Ren, Y.; Hu, Y.; Wang, J.; Jiang, L. Configurations and control of traction motors for electric vehicles: A review. *Chin. J. Electr. Eng.* **2017**, *3*, 1–17. [[CrossRef](#)]
- Tesla, I. *JTSLV00.0L13*; Certification Report; USA Environmental Protection Agency (EPA): Washington, DC, USA, 2017.
- Huynh, T.A.; Hsieh, M.F. Performance Analysis of Permanent Magnet Motors for Electric Vehicles (EV) Traction Considering Driving Cycles. *Energies* **2018**, *11*, 1385. [[CrossRef](#)]
- Gerada, D.; Xu, Z.; Huang, X.; Gerada, C. Fully-integrated high-speed IM for improving high-power marine engines. *IET Electr. Power Appl.* **2019**, *13*, 148–153. [[CrossRef](#)]
- Madonna, V.; Giangrande, P.; Galea, M. Electrical Power Generation in Aircraft: Review, Challenges, and Opportunities. *IEEE Trans. Transp. Electr.* **2018**, *4*, 646–659. [[CrossRef](#)]
- Senda, K.; Namikawa, M.; Hayakawa, Y. Electrical steels for advanced automobiles—core materials for motors, generators and high-frequency reactors. *JFE Steel Res. Dep. Tokyo Tech. Rep* **2004**, *4*. Available online: <http://www.jfe-steel.co.jp/en/research/report/004/pdf/004-12.pdf> (accessed on 8 May 2019).
- Gerada, D.; Huang, X.; Zhang, C.; Zhang, H.; Zhang, X.; Gerada, C. Electrical Machines for Automotive Electrically Assisted Turbocharging. *IEEE/ASME Trans. Mechatron.* **2018**, *23*, 2054–2065. [[CrossRef](#)]
- Tanaka, I.; Yashiki, H. Magnetic and Mechanical Properties of Newly Developed High-Strength Nonoriented Electrical Steel. *IEEE Trans. Magn.* **2010**, *46*, 290–293. [[CrossRef](#)]
- Caprio, M.T.; Lelos, V.; Herbst, J.; Manifold, S.; Jordon, H. High Strength Induction Machine, Rotor, Rotor Cage End Ring and Bar Joint, Rotor End Ring, and Related Methods. U.S. Patent 7,504,756, 17 March 2009.
- Gerada, D.; Mebarki, A.; Brown, N.L.; Bradley, K.J.; Gerada, C. Design Aspects of High-Speed High-Power-Density Laminated-Rotor Induction Machines. *IEEE Trans. Ind. Electr.* **2011**, *58*, 4039–4047. [[CrossRef](#)]

18. Caprio, M.T.; Lelos, V.; Herbst, J.D.; Upshaw, J. Advanced Induction Motor Endring Design Features for High Speed Applications. In Proceedings of the IEEE International Conference on Electric Machines and Drives, San Antonio, TX, USA, 15 May 2005; pp. 993–998. [[CrossRef](#)]
19. Alberti, L. A Modern Analysis Approach of Induction Motor for Variable Speed Application. Ph.D. Thesis, University of Padova, Padova, Italy, 2009. Available online: <http://paduaresearch.cab.unipd.it/> (accessed on 20 June 2019).
20. Alberti, L.; Bianchi, N.; Bolognani, S. Lamination Design of a Set of Induction Motors for Elevator Systems. In Proceedings of the IEEE International Electric Machines & Drives Conference (IEMDC '07), Antalya, Turkey, 3–5 May 2007; Volume 1, pp. 514–518. [[CrossRef](#)]
21. Alberti, L.; Bianchi, N.; Bolognani, S. A Very Rapid Prediction of IM Performance Combining Analytical and Finite-Element Analysis. *IEEE Trans. Ind. Appl.* **2008**, *44*, 1505–1512. [[CrossRef](#)]
22. Alberti, L.; Bianchi, N.; Boglietti, A.; Cavagnino, A. Core Axial Lengthening as Effective Solution to Improve the Induction Motor Efficiency Classes. *IEEE Trans. Ind. Appl.* **2014**, *50*, 218–225. [[CrossRef](#)]
23. Alberti, L.; Bianchi, N. A Coupled Thermal-Electromagnetic Analysis for a Rapid and Accurate Prediction of IM Performance. *IEEE Trans. Ind. Electr.* **2008**, *55*, 3575–3582. [[CrossRef](#)]
24. Staton, D.; Boglietti, A.; Cavagnino, A. Solving the More Difficult Aspects of Electric Motor Thermal Analysis in Small and Medium Size Industrial Induction Motors. *IEEE Trans. Energy Convers.* **2005**, *20*, 620–628. [[CrossRef](#)]
25. Bottesi, O.; Alberti, L.; Sabariego, R.V.; Gyselinck, J. A computational technique for iron losses in electrical machines. In Proceedings of the IEEE Energy Conversion Congress and Exposition (ECCE), Milwaukee, IL, USA, 18–22 September 2016; pp. 1–8. [[CrossRef](#)]
26. Bottesi, O.; Calligaro, S.; Alberti, L. Investigation on the frequency effects on iron losses in laminations. In Proceedings of the IEEE Energy Conversion Congress and Exposition (ECCE), Cincinnati, OH, USA, 1–5 October 2017; pp. 1161–1168. [[CrossRef](#)]
27. Concari, L.; Barater, D.; Concari, C.; Toscani, A.; Buticchi, G.; Liserre, M. H8 architecture for reduced common-mode voltage three-phase PV converters with silicon and SiC power switches. In Proceedings of the 43rd Annual Conference of the IEEE Industrial Electronics Society IECON, Beijing, China, 5–8 November 2017; pp. 4227–4232. [[CrossRef](#)]
28. Hava, A.; Un, E. Performance Analysis of Reduced Common-Mode Voltage PWM Methods and Comparison With Standard PWM Methods for Three-Phase Voltage-Source Inverters. *IEEE Trans. Power Electr.* **2009**, *24*, 241–252. [[CrossRef](#)]
29. Concari, L.; Barater, D.; Buticchi, G.; Concari, C.; Liserre, M. H8 Inverter for Common-Mode Voltage Reduction in Electric Drives. *IEEE Trans. Ind. Appl.* **2016**, *52*, 4010–4019. [[CrossRef](#)]
30. Concari, L.; Barater, D.; Toscani, A.; Franceschini, G.; Buticchi, G.; Liserre, M.; Zhang, H. Assessment of Efficiency and Reliability of Wide Band-gap based H8 Inverter in Electric Vehicle Applications. *Energies* **2019**, *12*, 1922. [[CrossRef](#)]
31. Barater, D.; Immovilli, F.; Soldati, A.; Buticchi, G.; Franceschini, G.; Gerada, C.; Galea, M. Multistress Characterization of Fault Mechanisms in Aerospace Electric Actuators. *IEEE Trans. Ind. Appl.* **2017**, *53*, 1106–1115. [[CrossRef](#)]
32. Rasilo, P.; Salem, A.; Abdallah, A.; De Belie, F.; Dupré, L.; Melkebeek, J.A. Effect of Multilevel Inverter Supply on Core Losses in Magnetic Materials and Electrical Machines. *IEEE Trans. Energy Convers.* **2015**, *30*, 736–744. [[CrossRef](#)]
33. Lee, W.; Schubert, E.; Li, Y.; Li, S.; Bobba, D.; Sarlioglu, B. Overview of Electric Turbocharger and Supercharger for Downsized Internal Combustion Engines. *IEEE Trans. Transp. Electr.* **2017**, *3*, 36–47. [[CrossRef](#)]
34. Lim, M.; Kim, J.; Hwang, Y.; Hong, J. Design of an Ultra-High-Speed Permanent-Magnet Motor for an Electric Turbocharger Considering Speed Response Characteristics. *IEEE/ASME Trans. Mechatron.* **2017**, *22*, 774–784. [[CrossRef](#)]
35. Ono, Y.; Shiraishi, K.; Yamashita, Y. Application of a Large Hybrid Turbocharger for Marine Electric-power Generation. *Mitsubishi Heavy Ind. Tech. Rev.* **2012**, *49*, 29–33.
36. Shiraishi, K.; Ono, Y.; Sakamoto, M. Energy Savings through Electric-assist Turbocharger for Marine Diesel Engines. *Mitsubishi Heavy Ind. Tech. Rev.* **2015**, *52*, 36–41.

37. Gerada, D.; Mebarki, A.; Brown, N.L.; Gerada, C.; Cavagnino, A.; Boglietti, A. High-Speed Electrical Machines: Technologies, Trends, and Developments. *IEEE Trans. Ind. Electr.* **2013**, *61*, 2946–2959. [[CrossRef](#)]
38. Gerada, D.; Xu, Z.; Golovanov, D.; Gerada, C. Comparison of electrical machines for use with a high-horsepower marine engine turbocharger. In Proceedings of the 25th International Workshop on Electric Drives: Optimization in Control of Electric Drives (IWED), Moscow, Russia, 31 January–2 February 2018; pp. 1–6. [[CrossRef](#)]
39. *IEEE Standard Test Procedure for Polyphase Induction Motors and Generators*; IEEE: Piscataway, NJ, USA, 2018.



© 2019 by the authors. Licensee MDPI, Basel, Switzerland. This article is an open access article distributed under the terms and conditions of the Creative Commons Attribution (CC BY) license (<http://creativecommons.org/licenses/by/4.0/>).